Vision-Based Tracking for Unmanned Aerial Vehicles

Vilas K. Chitrakaran, Darren M. Dawson, Hariprasad Kannan, and Matthew Feemster

Abstract

This paper presents the design of a vision-based controller for an underactuated, unmanned aerial vehicle (UAV) equipped with a pan-tilt camera unit (PTCU) to achieve the objective of following a leader vehicle autonomously. The relative position and orientation information is obtained from the monocular camera utilizing homography-based techniques. The proposed controller, built upon Lyapunov design methods, achieves uniform ultimate bounded (UUB) tracking. As an extension, it is also demonstrated that the approach used in the development of the control strategy for the leader-follower problem can be applied, with a few modifications, to the problem of trajectory tracking, where the desired trajectory is described as a sequence of images taken, for example, by the on-board camera during a previous flight.

Index Terms

Unmanned aerial vehicles, visual servo control, autonomous systems, Lyapunov analysis.

Manuscript submitted for consideration as regular paper.

V. K. Chitrakaran, D. M. Dawson and H. Kannan are with Clemson University. M. Feemster is with the United States Naval Academy. Corresponding author: V. K. Chitrakaran, Email: vilas@ieee.org, Fax: +1-864-656-7218, Address: 315, EIB, ECE Dept. Clemson University, Clemson, SC, 29634, USA.

Vision-Based Tracking for Unmanned Aerial Vehicles

I. Introduction

THE advantages of employing UAVs in dangerous and unstructured environments have already made them an essential component in various civilian tasks such as disaster related search and rescue, terrain mapping and aerial surveillance, as well as in modern warfare. Fueled by the recent availability of low-cost hardware such as remotely radio-controlled electric and gas powered helicopters and fixed-wing aircrafts, numerous research groups are currently working towards developing novel applications and control strategies for UAVs. Among the most popular is the quad-rotor helicopter design, chiefly due to its design simplicity and high maneuverability. New studies aimed at developing high-performance quad-rotor helicopters have appeared in recent publications [22], and provides insights to various stability problems and control challenges involved [18]. These vehicles are underactuated, *i.e.*, they are not equipped with sufficient actuators that allow independent translation and rotation about any given direction. In [2], the authors proposed a controller design based on feedback linearization technique, where the performance of a hybrid controller capable of switching between multiple modes of UAV flight (such as take-off, hover, landing, and so on) was demonstrated. However, due to the coupled nature of the translational and rotational dynamics of a quad-rotor, the most common control design technique employed, including in this paper, is the backstepping approach.

In addition to control design challenges, there exists the problem of accurate measurement of position and orientation in such machines. To this end, vision sensors are being increasingly utilized within the feedback loop of such systems. An off-board vision system and a fixed camera were used in [2] in order to estimate the position and orientation of the UAV by tracking artificially embedded visual features on the UAV. In a subsequent work [3], the authors also proposed the use of multiple cameras (a pan-tilt unit on the ground and a camera on-board, in line of sight of each other) in an effort to improve the accuracy of position estimation. Experimental results for different approaches to utilizing vision in position sensing in helicopters have also appeared in [21], [23]. One of the difficulties associated with visual servoing is to ensure that the target features remain within the field of view of the camera at all times. Metni *et al.* [20] proposed a controller with bounds imposed on the UAV orientation using saturation functions, in an effort to maintain the direction of the optical axis of the camera fixed on the UAV as close as possible to the direction of the visual targets, hence, keeping the targets within the field of view. Active control of pan-tilt cameras have also been proposed [9], [25] to help maintain view of targets. Visual servo controllers usually fall into one of the following two classes - image-based visual servoing (IBVS), and position-based visual servoing (PBVS) [11], depending upon whether the controller is designed to directly act on the visual information (*i.e.*, in image space), or whether the visual information is first utilized in the estimation of the Euclidean pose, respectively. An IBVS scheme was presented in [15] where the dynamics of features in image space were formulated in terms of their spherical projections (a spherical image surface as opposed to planar). A relatively recent development is the homography-based approach to visual servoing (also called $2\frac{1}{2}$D visual servoing [17]), which utilizes a combination of partially reconstructed Euclidean information and 2D image-space information in the control design, and has been shown to have many practical advantages. As mentioned in [17], this method does not require an accurate Euclidean model of the environment, and potential singularities in the image Jacobian are avoided. The homography matrix is computed from two views - a reference image and images captured online from a moving camera. Decomposition of the homography matrix provides information about the motion of the camera between the two views in terms of a rotation matrix and a translation vector that is scaled by the distance between the targets and camera at the reference position. Usually, this constant scale factor is unknown in a visual servoing task, and hence, must be estimated online if required in the control design. In [6], an adaptive estimation technique was utilized to compensate for this unknown depth information in the visual servoing of a wheeled mobile robot. The idea presented in [6] was subsequently extended to the problem of trajectory tracking for a UAV by other researchers [19].

In a preliminary version of this work presented in [7], we utilized the image information from a monocular camera fixed to the body frame of a quad-rotor UAV to develop a controller for landing the UAV autonomously. The position and orientation errors were formulated by comparing the stream of images captured from the on-board camera to a previously acquired reference image taken by the camera when the UAV was at the desired final position and orientation on the landing pad. Hence, if the images from the camera match the desired reference image, the control objective will have been achieved. However, due to the underactuated nature of the aircraft, the orientation of the UAV cannot always be controlled to guarantee that both the images will match, since two out of the three rotational degrees of freedom (d.o.f) are lost in achieving the position objective. In this paper, we utilize a pan-tilt camera on the UAV to eliminate this problem. With the two additional rotational d.o.f offered by the PTCU, the combined UAV-PTCU system can be controlled such that the desired and actual images from the camera coincide. With this new modification to the vision system, we extend our previous

work towards the development of a vision-based controller for a UAV to autonomously follow a leader vehicle (*e.g.* another aircraft or a ground vehicle). The relative position and orientation between the leader and the camera frame on the follower are obtained by comparing the images captured by the camera on the follower with a reference image of the leader captured apriori. The error signals are formulated such that the unknown scale factor, resulting from the decomposition of the homography matrix, is not directly utilized in the control design. Similar to the approach followed in [1] and [7], a constant design vector is integrated into the controller, resulting in an input matrix that facilitates an advantageous coupling of translational dynamics of the UAV to the rotational torque inputs. In Appendix I, it is shown that the leader-follower strategy can also be adapted to vision-based trajectory tracking, where the desired trajectory of the UAV is defined in terms of a sequence of images of stationary features on the ground, captured, for example, during a previous flight of the UAV. The approach proposed in this paper has many advantages relative to similar work in the literature. Only a single camera is utilized for visual sensing. The controller on the follower UAV does not require any information from the leader, such as leader velocity or acceleration. A model describing the motion of the leader vehicle is not required. Also, a camera mounted on a pan-tilt unit is more effective in maintaining line of sight with feature points on the leader vehicle compared to a body fixed camera with a limited field of view.

II. System Model

Our development platform is a quad-rotor helicopter. The vehicle, shown in Figure 1, is a four rotor aircraft capable of vertical take-off and landing (VTOL). In the figure, the pan-tilt camera unit (PTCU) is shown mounted on the forward-looking limb of the aircraft. However, for the sake of simplicity in the subsequent development, we will assume that the optical center of the camera coincides with the origin of the body fixed frame on the UAV. The camera is mounted such that the optical axis of the camera points down along the z axis of the UAV body fixed frame when pan and tilt angles are zero. We will adhere to the following convention, borrowed from Fossen [5], throughout the paper: vector quantities denoting UAV position and velocity are specified as v^n_{eb}, which denotes the vector quantity v associated with the b frame defined relative to the e frame, and expressed in n frame. We use 'x', 'v', and 'ω' to denote position, translational velocity and angular velocity, respectively. Rotation matrices are specified as $R^t_f \in SO(3)$ denotes a 3×3 matrix that transforms coordinates defined in f frame to t frame.

A. Dynamic Model of a UAV

The UAV that we are considering is fully actuated with respect to orientation but underactuated with respect to translation (*i.e.*, the UAV is equipped with only one control input (the thrust force) to facilitate translational motion). The control development is focused on the rigid body dynamics of the UAV (*i.e.*, actuator dynamics are not considered within the scope of the design). After denoting I and F as the inertial frame and the follower UAV body fixed frame, respectively, the rigid body dynamics are described by the following equations [10]

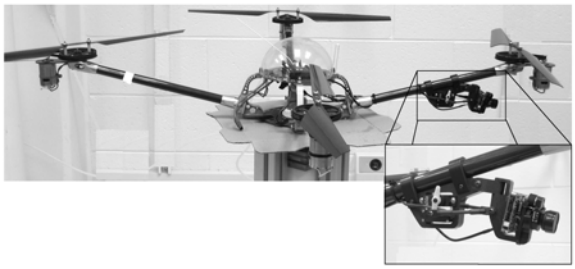

Fig. 1. A 'Draganflyer' quad-rotor aircraft with an on-board pan-tilt camera.

$$\dot{x}^F_{IF} = R^I_F v^F_{IF}, \quad (1)$$

$$m\dot{v}^F_{IF} = -mS\left(\omega^F_{IF}\right) v^F_{IF} + N_1(\cdot) + F^F_f, \quad (2)$$

$$\dot{R}^I_F = R^I_F S\left(\omega^F_{IF}\right), \quad (3)$$

$$M\dot{\omega}^F_{IF} = -S\left(\omega^F_{IF}\right) M\omega^F_{IF} + N_2(\cdot) + F^F_t \quad (4)$$

where $S(\cdot) \in \mathbb{R}^{3\times3}$ denotes a skew-symmetric matrix defined in [24], $M \in \mathbb{R}^{3\times3}$ denotes the constant moment of inertia around the center of mass expressed in body frame F, and $m \in \mathbb{R}^1$ represents the constant mass of the UAV. The term $N_1\left(v^F_{IF}, R^I_F, t\right) \in \mathbb{R}^3$ represents the sum of gravitational forces and additional time varying unmodeled bounded dynamics such as aerodynamic resistance. Similarly, the term $N_2\left(v^F_{IF}, \omega^F_{IF}, R^I_F, t\right) \in \mathbb{R}^3$ includes unmodeled, bounded disturbances within the rotational dynamics. The forces and torques on the rigid body due to the actuators are denoted by $F^F_f(t), F^F_t(t) \in \mathbb{R}^3$, respectively, expressed in the body frame F, and given as follows

$$F^F_f = \begin{bmatrix} 0 & 0 & u_1 \end{bmatrix}^T, \quad (5)$$

$$F^F_t = \begin{bmatrix} u_2 & u_3 & u_4 \end{bmatrix}^T \quad (6)$$

where $u_i(t) \in \mathbb{R}^1$ denote the four scalar signals that are used to control the UAV.

Remark 1: The four rotor velocities $\varpi_i \in \mathbb{R}^1$ of a quad-rotor UAV are related to the rigid body forces $F^F_f(t)$ and torques $F^F_t(t)$ via the following relationship [10]

$$\begin{bmatrix} u_1 \\ u_2 \\ u_3 \\ u_4 \end{bmatrix} = \begin{bmatrix} -b & -b & -b & -b \\ 0 & db & 0 & -db \\ db & 0 & -db & 0 \\ k & -k & k & -k \end{bmatrix} \begin{bmatrix} \varpi_1^2 \\ \varpi_2^2 \\ \varpi_3^2 \\ \varpi_4^2 \end{bmatrix} \quad (7)$$

where $d \in \mathbb{R}^1$ denotes the displacement of each rotor relative to the center of mass of the airframe, and $k, b \in \mathbb{R}^1$ are constant parameters that depend on the construction and aerodynamic properties of the rotor blades.

B. Kinematics of the Pan-Tilt Camera Unit

The PTCU is mounted on the UAV such that the camera frame, denoted by C, coincides with the UAV frame F when the pan and tilt angles, denoted by $\theta_p(t), \theta_t(t) \in \mathbb{R}$, respectively, are zero. At this configuration, the optical axis of the camera points down along the z axis of the UAV. Based

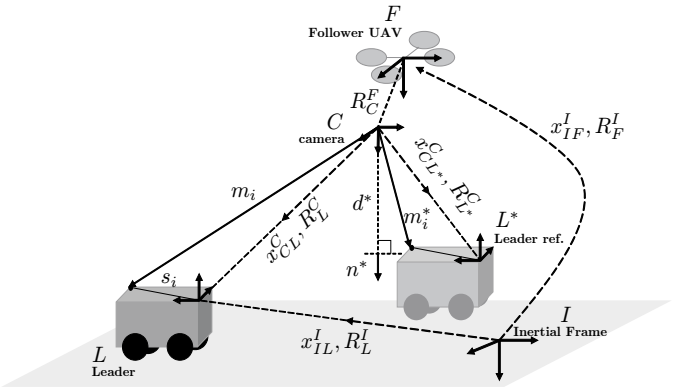

Fig. 2. Coordinate frame assignments and geometrical relationships.

on this geometry, the standard Denavit-Hartenberg procedure [24] can be applied to compute the camera kinematics relative to the UAV as follows

$$R_C^F = \begin{bmatrix} \mathrm{c}(\theta_t) & 0 & \mathrm{s}(\theta_t) \\ \mathrm{s}(\theta_p)\mathrm{s}(\theta_t) & \mathrm{c}(\theta_p) & -\mathrm{s}(\theta_p)\mathrm{c}(\theta_t) \\ -\mathrm{c}(\theta_p)\mathrm{s}(\theta_t) & \mathrm{s}(\theta_p) & \mathrm{c}(\theta_p)\mathrm{c}(\theta_t) \end{bmatrix} \quad (8)$$

$$\omega_{FC}^F = \begin{bmatrix} 1 & 0 \\ 0 & \mathrm{c}(\theta_p) \\ 0 & \mathrm{s}(\theta_p) \end{bmatrix} \begin{bmatrix} \dot{\theta}_p \\ \dot{\theta}_t \end{bmatrix} = J_c \dot{\theta}_c, \quad (9)$$

$$\dot{R}_C^F = S\left(\omega_{FC}^F\right) R_C^F \quad (10)$$

where $c(\theta), s(\theta) \in \mathbb{R}^1$ represent the sine and cosine, respectively, and $J_c(t) \in \mathbb{R}^{3\times 2}$ denotes the Jacobian for the PTCU.

Remark 2: In the subsequent development, we will assume that the dynamics of the PTCU can be ignored (*i.e.*, the pan and tilt angular velocities, denoted by $\dot{\theta}_c(t)$, are directly related to the respective actuator inputs by proportionality constants only).

C. Vision System Model

The geometric relationships between the leader and the follower vehicles are shown in Figure 2. As mentioned previously, the origins of the camera frame C and the follower UAV frame F coincide; however, these frames are shown separate in the figure for the sake of clarity. The leader vehicle, whose body fixed frame is denoted by L, is augmented with coplanar features whose image coordinates can be easily tracked by processing the video stream from the camera mounted on the follower UAV. Let the constant vector $s_i \in \mathbb{R}^3$ expressed in the leader frame L define the coordinates of the i^{th} feature on the leader vehicle, and let $m_i(t) = \begin{bmatrix} x_i(t) & y_i(t) & z_i(t) \end{bmatrix}^T \in \mathbb{R}^3$ denote the Euclidean coordinates of the same feature defined in the follower UAV's camera frame C. The frame L^* in Figure 2 denotes the leader at the desired position and orientation relative to the camera frame on the follower, denoted by $x_{CL^*}^C \in \mathbb{R}^3$ and $R_{L^*}^C \in SO(3)$, respectively, and $m_i^* \in \mathbb{R}^3$denotes the constant Euclidean coordinates of the i^{th} feature point relative to the camera at this position. Based on geometry of Figure 2, the expressions for $m_i(t)$ and m_i^* are as follows

$$m_i = x_{CL}^C + R_L^C s_i, \quad (11)$$

$$m_i^* = x_{CL^*}^C + R_{L^*}^C s_i. \quad (12)$$

After solving (12) for s_i and then substituting the resulting expression into (11), we have

$$m_i = \bar{x} + \bar{R} m_i^* \quad (13)$$

where $\bar{R}(t) \in SO(3)$ and $\bar{x}(t) \in \mathbb{R}^3$ are defined as follows

$$\bar{R} = R_L^C R_C^{L^*}, \quad (14)$$

$$\bar{x} = x_{CL}^C - \bar{R} x_{CL^*}^C. \quad (15)$$

In Figure 2, $n^* \in \mathbb{R}^3$ denotes the constant normal to the plane of features on the leader at desired relative position, expressed in the camera frame C, and the constant $d^* \neq 0 \in \mathbb{R}^1$ denotes the distance of this plane from the camera. It can be seen from Figure 2 that the projection of m_i^* for all features along the unit normal n^* is given by

$$d^* = n^{*T} m_i^*. \quad (16)$$

Using (16), the relationship in (13) can be written in terms of a Euclidean homography $H(t) \in \mathbb{R}^{3\times 3}$ [14] relating the coordinates $m_i(t)$ and m_i^* as follows

$$m_i = \underbrace{\left(\bar{R} + \frac{1}{d^*}\bar{x} n^{*T}\right)}_{H} m_i^*. \quad (17)$$

The measurable 2D homogeneous image coordinates of the features, denoted by $p_i(t), p_i^* \in \mathbb{R}^3$, expressed in the coordinates of frame C, are related to the normalized Euclidean coordinates $\frac{m_i(t)}{z_i(t)}$ and $\frac{m_i^*}{z_i^*}$, respectively, by the pin-hole camera model [14] such that

$$p_i = A\frac{m_i}{z_i}, \qquad p_i^* = A\frac{m_i^*}{z_i^*} \quad (18)$$

where $A \in \mathbb{R}^{3\times 3}$ is a known, constant, upper triangular and invertible intrinsic camera calibration matrix, and $z_i(t), z_i^* \in \mathbb{R}^1$ are the third coordinate elements in the vectors $m_i(t)$ and m_i^*, respectively. Hence, the relationship in (17) can now be expressed in terms of image coordinates of the features as follows

$$p_i = \underbrace{\frac{z_i^*}{z_i}}_{\alpha_i} \underbrace{A\left(\bar{R} + \frac{1}{d^*}\bar{x} n^{*T}\right) A^{-1}}_{G} p_i^* \quad (19)$$

where $\alpha_i(t) \in \mathbb{R}^1$ denotes the depth ratio $\frac{z_i^*}{z_i(t)}$ and $G(t) \in \mathbb{R}^{3\times 3}$ is a full rank homogeneous collineation matrix [14]. Given pairs of correspondences $(p_i(t), p_i^*)$ for a minimum of four coplanar non-collinear features on the leader, the set of linear equations in (19) can be solved to compute a unique $G(t)$ up to a scale factor [14]. When more than four feature point correspondences are available, $G(t)$ can also be recovered (again, up to a scale factor) using techniques such as least-squares minimization. $G(t)$ can then be used to uniquely determine $H(t)$, taking into account the fact that the intrinsic camera calibration matrix A is assumed to be known [14]. By

utilizing the algorithms described in [4], [14], $H(t)$ can be decomposed to recover the rotational component $\bar{R}(t)$ and the scaled translational component $\frac{1}{d^*}\bar{x}(t)$. The signals $\bar{R}(t)$ and $\frac{1}{d^*}\bar{x}(t)$ are the measurable quantities from the vision system that we will exploit to design a controller for the follower UAV.

Remark 3: If all the features on the leading vehicle are not coplanar, the collineation matrix in (19) can still be developed by employing the virtual parallax algorithm described in [17]. However, in this case, at least eight non-coplanar features must be utilized.

Remark 4: Decomposition of the Homography matrix $H(t)$ results in four unique solutions, two of which are physically impossible. From the remaining two solutions, the right one can be selected by utilizing some additional information, such as a guess for the normal vector n^*.

III. Control Formulation

The control objective is to ensure that the follower UAV and the PTCU are controlled such that the images of the features on the leader, seen by the camera on the follower, matches the reference image of the same features captured by the camera when the leader is at a desired relative position and orientation. Based on Figure 2 and the development in the previous section, this can be stated as the desire to control the follower UAV such that the following control objective is achieved

$$x_{CL}^C \to x_{CL^*}^C, R_L^C \to R_{L^*}^C \quad \text{as } t \to \infty. \tag{20}$$

An examination of equations (14) and (15) reveals that the control objective stated above can be achieved if the follower UAV and the PTCU can be controlled such that $\bar{R}(t) \to I_{3\times 3}$ and $\bar{x}(t) \to 0$ as $t \to \infty$, where the notation $I_{n\times n}$ denotes an $n \times n$ identity matrix. To achieve the stated objective, we make the following assumptions

Assumption 1: The velocities $v_{IF}^F(t)$ and $\omega_{IF}^F(t)$ are measurable from inertial sensors on-board the follower UAV.

Assumption 2: The uncertain nonlinearties in the UAV translational and rotational dynamics, denoted by $N_1(\cdot)$ and $N_2(\cdot)$ in (2) and (4), respectively, can be upperbounded in the following manner

$$\|N_1\| \leq \psi_1\left(\left\|v_{IF}^F\right\|\right) \tag{21}$$

$$\|N_2\| \leq \psi_2\left(\left\|v_{IF}^F\right\|, \left\|\omega_{IF}^F\right\|\right) \tag{22}$$

where $\psi_i(\cdot) \in \mathbb{R}^1$ are positive, scalar, non-decreasing functions of their arguments.

Assumption 3: The pan and tilt angles of the camera are measurable from the resolvers in the PTCU. We also assume that the dynamics of the PTCU can be ignored, *i.e.*, the angular velocities of the pan and tilt angles of the PTCU can be directly controlled.

Assumption 4: The pan angle of the camera is confined to the region $\frac{-\pi}{2} < \theta_p(t) < \frac{\pi}{2}$.

Assumption 5: The scaled position and orientation variables $\frac{1}{d^*}\bar{x}(t)$ and $\bar{R}(t)$ are available from the vision system.

Assumption 6: The position and velocities of the leader vehicle are bounded, *i.e.*, $x_{IL}^I(t), v_{IL}^I(t), \omega_{IL}^I(t) \in \mathcal{L}_\infty$. However, these signals are not available to the controller on the follower UAV, *i.e.*, there is no communication between the vehicles.

Assumption 7: The features on the leader are in front of the camera on the follower (*i.e.*, $z_i > \gamma$ for every feature point, where $\gamma \in \mathbb{R}^1$, is a positive scalar constant), and the features on the leader remain within the field of view of the camera on the follower.

A. Orientation Error Formulation

The axis-angle representation [24] of the rotation matrix $\bar{R}(t)$ defined in (14) is utilized to define the orientation error, denoted by $e_\theta(t) \in \mathbb{R}^3$, as follows

$$e_\theta \triangleq \mu\phi \tag{23}$$

where $\mu(t) \in \mathbb{R}^3$ represents a unit axis of rotation, and $\phi(t) \in \mathbb{R}^1$ denotes the rotation angle about $\mu(t)$ (confined to the region $-\pi < \phi(t) < \pi$), explicitly defined as follows

$$\phi = \cos^{-1}\left(\frac{1}{2}\left(\text{tr}(\bar{R}) - 1\right)\right), \quad S(\mu) = \frac{\bar{R} - \bar{R}^T}{2\sin(\phi)} \tag{24}$$

where the notation $\text{tr}(\cdot)$ denotes the trace of a matrix. After taking the time derivative of the orientation error system in (23), and utilizing the PTCU kinematics from (9), the open loop dynamics for the orientation error system can be expressed as follows

$$\begin{aligned} \dot{e}_\theta &= L_\omega \omega_{CL}^C \\ &= -L_\omega R_F^C \omega_{IF}^F - L_\omega R_F^C J_c \dot{\theta}_c + L_\omega \omega_{IL}^C \end{aligned} \tag{25}$$

where $L_\omega(t) \in \mathbb{R}^{3\times 3}$ is a Jacobian-like matrix given by the following expression

$$\begin{aligned} L_\omega &= I_{3\times 3} - \frac{\phi}{2}S(\mu) + \left(1 - \frac{sinc(\phi)}{sinc^2\left(\frac{\phi}{2}\right)}\right) S(\mu)^2, \\ sinc(\phi) &\triangleq \frac{\sin(\phi)}{\phi}. \end{aligned} \tag{26}$$

The development of the expression for $L_\omega(t)$ is presented in detail in [8] and [16], and utilizes the time derivative of (14), which provides an expression for the time derivative of $\bar{R}(t)$ as follows

$$\dot{\bar{R}} = S\left(\omega_{CL}^C\right)\bar{R} \tag{27}$$

where the following property was utilized in its derivation

$$\dot{R}_L^C = S\left(\omega_{CL}^C\right) R_L^C. \tag{28}$$

Remark 5: By exploiting the fact that $\mu(t)$ is a unit vector (*i.e.*, $\|\mu\|^2 = 1$), the determinant of $L_\omega(t)$ can be derived as follows [16]

$$\det\{L_\omega\} = \frac{1}{sinc^2\left(\frac{\phi}{2}\right)}. \tag{29}$$

From (29), it can be seen that $\det\{L_\omega(t)\}$ is non-zero and finite everywhere except at multiples of 2π, which is outside the assumed range for $\phi(t)$. $L_\omega(t)$ is assumed invertible in the subsequent development.

B. Position Error Formulation

The position error is denoted by $\bar{x}_h(t) \in \mathbb{R}^3$, and defined as follows

$$\bar{x}_h \triangleq \frac{1}{d^*}\bar{x}. \tag{30}$$

The open loop dynamics of the position error system can be obtained by taking the time derivative of (15) as follows

$$d^* \dot{\bar{x}}_h = \dot{x}^C_{CL} - \dot{\bar{R}}\, x^C_{CL^*}. \tag{31}$$

From the geometry in Figure 2, it can be seen that

$$x^C_{CL} = R^C_F R^F_I \left(x^I_{IL} - x^I_{IF}\right) \tag{32}$$

and the time derivative of (32), after simplification, can be expressed as follows

$$\dot{x}^C_{CL} = -R^C_F v^F_{IF} - S\left(\omega^C_{IC}\right) x^C_{CL} + v^C_{IL} \tag{33}$$

where (3) and (10) have been utilized. After substituting (33) in (31), and utilizing (27) for the time derivative of $\bar{R}(t)$, the following expression for the open loop position error dynamics can be obtained

$$\begin{aligned} d^* \dot{\bar{x}}_h &= -R^C_F v^F_{IF} - S\left(\omega^C_{IC}\right) d^* \bar{x}_h \\ &\quad -S\left(\omega^C_{IL}\right) \bar{R} x^C_{CL^*} + v^C_{IL}. \end{aligned} \tag{34}$$

Based on the subsequent Lyapunov stability analysis, an auxiliary signal $r(t) \in \mathbb{R}^6$ is defined as follows

$$r \triangleq \begin{bmatrix} r_p^T & e_\theta^T \end{bmatrix}^T \tag{35}$$

where $e_\theta(t)$ is the orientation error defined in (23), and $r_p(t) \in \mathbb{R}^3$ is defined in the following manner

$$r_p \triangleq k_p \bar{x}_h - R^C_F v^F_{IF} + R^C_F \delta \tag{36}$$

where $k_p \in \mathbb{R}^1$ denotes a positive, scalar constant, and $\delta = \begin{bmatrix} \delta_1 & \delta_2 & \delta_3 \end{bmatrix}^T \in \mathbb{R}^3$ represents a constant design vector. The constant δ introduced in (36) facilitates an advantageous coupling between the translational and rotational dynamics of the UAV. Upon substituting (36) in (34), the following alternate expression for the open loop position error dynamics is obtained

$$\begin{aligned} d^* \dot{\bar{x}}_h &= r_p - k_p \bar{x}_h - R^C_F \delta - S\left(\omega^C_{IC}\right) d^* \bar{x}_h \\ &\quad -S\left(\omega^C_{IL}\right) \bar{R} x^C_{CL^*} + v^C_{IL}. \end{aligned} \tag{37}$$

After taking the time derivative of (35), and substituting (34) for $\dot{\bar{x}}_h\ (t)$, the dynamics in (2) for $\dot{v}^F_{IF}(t)$, (10) for $\dot{R}^C_F(t)$, and (25) for $\dot{e}_\theta(t)$, the following expression for the open loop dynamics of $r(t)$ can be developed after some mathematical manipulation and simplification

$$\begin{aligned} \dot{r} &= \begin{bmatrix} -S\left(\omega^C_{IC}\right) r_p \\ 0_{3\times 1} \end{bmatrix} + \begin{bmatrix} R^C_F S\left(\omega^F_{IF}\right) \delta - \frac{1}{m} R^C_F F^F_f \\ -L_\omega R^C_F \omega^F_{IF} - L_\omega R^C_F J_c \dot{\theta}_c \end{bmatrix} \\ &\quad + N_{11} + N_{12} \end{aligned} \tag{38}$$

where $0_{n\times m}$ denotes a $n \times m$ zero matrix, and $N_{11}(t), N_{12}(t) \in \mathbb{R}^6$ groups the following terms in (38)

$$N_{11} \triangleq \begin{bmatrix} -\frac{k_p}{d^*} R^C_F v^F_{IF} - \frac{1}{m} R^C_F N_1 \\ 0_{3\times 1} \end{bmatrix}, \tag{39}$$

$$N_{12} \triangleq \begin{bmatrix} -\frac{k_p}{d^*} S\left(\omega^C_{IL}\right) \bar{R} x^C_{CL^*} + \frac{k_p}{d^*} v^C_{IL} \\ L_\omega \omega^C_{IL} \end{bmatrix}. \tag{40}$$

The second term in (38), after re-arrangement, can be written as the product of a matrix $\bar{B}(t) \in \mathbb{R}^{6\times 6}$ and a vector $\bar{U}(t) \in \mathbb{R}^6$, where

$$\bar{B} = B_1 B_2, \tag{41}$$

$$B_1 = \begin{bmatrix} -R^C_F & 0_{3\times 3} \\ 0_{3\times 3} & -L_\omega R^C_F \end{bmatrix}, \tag{42}$$

$$B_2 = \begin{bmatrix} 0 & 0 & -\delta_3 & \delta_2 & 0 & 0 \\ 0 & \delta_3 & 0 & -\delta_1 & 0 & 0 \\ \frac{1}{m} & -\delta_2 & \delta_1 & 0 & 0 & 0 \\ 0 & 1 & 0 & 0 & 1 & 0 \\ 0 & 0 & 1 & 0 & 0 & \mathrm{c}(\theta_p) \\ 0 & 0 & 0 & 1 & 0 & \mathrm{s}(\theta_p) \end{bmatrix}, \tag{43}$$

$$\bar{U} = \begin{bmatrix} u_1 \\ \omega^F_{IF} \\ \dot{\theta}_c \end{bmatrix}. \tag{44}$$

Hence, from (38), and (41) through (44), it can be shown that

$$\dot{r} = \begin{bmatrix} -S\left(\omega^C_{IC}\right) r_p \\ 0_{3\times 1} \end{bmatrix} + \bar{B}\bar{U} + N_{11} + N_{12}. \tag{45}$$

Remark 6: The matrix $B_2(t)$ is invertible if $\delta_3 \neq 0$ and at least one of δ_1 or δ_2 is non-zero. Since $B_1(t)$ is invertible, it follows that $\bar{B}(t)$ is invertible if δ is selected to satisfy the above mentioned constraints.

IV. Control Design

The control design is based on the backstepping technique. An auxiliary control signal $\bar{U}_n(t) \in \mathbb{R}^6$ and an angular velocity backstepping error signal $\eta(t) \in \mathbb{R}^3$ are defined as follows

$$\bar{U}_n = \begin{bmatrix} u_1 & \omega_n^T & \dot{\theta}_c^T \end{bmatrix}^T, \tag{46}$$

$$\eta = \left[\omega_n - \omega^F_{IF}\right]^T \tag{47}$$

where $\omega_n(t) \in \mathbb{R}^3$ represents a desired angular velocity signal. From (44), (46) and (47), the following relationship can be observed

$$\bar{U} = \bar{U}_n - \Pi^T \eta \tag{48}$$

where $\Pi \in \mathbb{R}^{3\times 6}$ denotes the following constant matrix

$$\Pi = \begin{bmatrix} 0 & 1 & 0 & 0 & 0 & 0 \\ 0 & 0 & 1 & 0 & 0 & 0 \\ 0 & 0 & 0 & 1 & 0 & 0 \end{bmatrix}. \tag{49}$$

The auxiliary control input $\bar{U}_n(t)$ is designed in the following manner

$$\bar{U}_n = \bar{B}^{-1} U \tag{50}$$

where $U(t) \in \mathbb{R}^6$ is a subsequently designed control input. From (45), (48) and (50), the open loop dynamics for $r(t)$ can now be expressed as follows

$$\dot{r} = \begin{bmatrix} -S\left(\omega^C_{IC}\right) r_p \\ 0_{3\times 1} \end{bmatrix} + U + \bar{B}\Pi^T \eta + N_{11} + N_{12}. \tag{51}$$

Similarly, after differentiating (47) and substituting for $\dot{\omega}^F_{IF}(t)$ from the UAV rotational dynamics given by (4), the open loop dynamics for the angular velocity error signal $\eta(t)$ are obtained as follows

$$M\dot{\eta} = M\Pi\dot{\bar{U}}_{n1} + S\left(\omega^F_{IF}\right) M \omega^F_{IF} - N_{22} - F^F_t \tag{52}$$

where the measurable and unmeasurable terms have been grouped into $\dot{\bar{U}}_{n1}(t) \in \mathbb{R}^3$ and $\dot{\bar{U}}_{n2}(t) \in \mathbb{R}^3$, respectively (See Appendix II for explicit derivations), and finally, all unmeasurable terms in the rotational dynamics have been combined into a single term $N_{22}(t) \in \mathbb{R}^3$ defined in the following manner

$$N_{22} \triangleq N_2 - M\Pi\dot{\bar{U}}_{n2}. \tag{53}$$

From Assumption 2, (39) and (53), it is easy to see that the uncertain terms $N_{11}(t)$ and $N_{22}(t)$ can be upperbounded in the following manner

$$\|N_{11}\| \leq \zeta_1\left(\left\|v_{IF}^F\right\|_s\right) \tag{54}$$
$$\|N_{22}\| \leq \zeta_2\left(\left\|v_{IF}^F\right\|, \left\|\omega_{IF}^F\right\|\right) \tag{55}$$

where $\zeta_i(\cdot) \in \mathbb{R}^1$ are positive, scalar, non-decreasing functions of their arguments. The subsequent control design requires that $\zeta_1(\cdot)$ be differentiable, and hence, it is constructed as a function of a modified norm, denoted by $\|\cdot\|_s$, which is defined in the following manner

$$\|y\|_s \triangleq \sqrt{y^T y + \sigma},\ \forall y \in \mathbb{R}^3 \tag{56}$$

where $\sigma \in \mathbb{R}^1$ represents a small positive constant. Based on the stability analysis presented in the next sub-section, the control inputs $U(t)$ and $F_t^F(t)$ are designed as follows

$$U = -k_r r - \begin{bmatrix} \bar{x}_h \\ 0_{3\times 1} \end{bmatrix} - r\frac{\zeta_1^2}{\varepsilon_1}, \tag{57}$$
$$F_t^F = M\Pi\dot{\bar{U}}_{n1} + S\left(\omega_{IF}^F\right) M\omega_{IF}^F + k_\eta \eta - \Pi\bar{B}^T r + \eta\frac{\zeta_2^2}{\varepsilon_2} \tag{58}$$

where $k_r, k_\eta \in \mathbb{R}^1$ are positive, scalar control gains, $\varepsilon_1, \varepsilon_2 \in \mathbb{R}^1$ are positive, scalar constants.

Remark 7: The function in (56) is utilized in (54) instead of the standard Euclidean norm to ensure that the time derivative of $\zeta_1(\cdot)$, which appears in $\dot{\bar{U}}_{n1}(t)$ in (58), is well-defined. The time derivative of $\|\cdot\|_s$ is expressed as follows

$$\frac{d}{dt}\|y\|_s = \frac{y^T\dot{y}}{\sqrt{y^T y + \sigma}},\ \forall y \in \mathbb{R}^3. \tag{59}$$

A. Stability Analysis

Theorem 1: Given the error dynamics of (37), (51) and (52), the translational force input and the rotational torque input developed in (57) and (58), respectively, guarantees uniform ultimate boundededness (UUB) in the position error signal $\bar{x}_h(t)$ and the orientation error signal $e_\theta(t)$ in a neighborhood about zero, in the sense that

$$\|\bar{x}_h(t)\|, \|e_\theta(t)\| \leq \alpha_1 \exp\left(-\alpha_2 t\right) + \alpha_3 \tag{60}$$

where $\alpha_1, \alpha_2, \alpha_3 \in \mathbb{R}^1$ are adjustable, positive constants.

Proof: We choose the following non-negative scalar function as the Lyapunov candidate to prove the above theorem

$$V \triangleq \frac{1}{2}d^*\bar{x}_h^T\bar{x}_h + \frac{1}{2}r^T r + \frac{1}{2}\eta^T M\eta. \tag{61}$$

After taking the time derivative of (61), substituting the dynamics for $\dot{\bar{x}}_h(t), \dot{r}(t)$ and $\dot{\eta}(t)$ from (37), (51) and (52), and substituting the expressions for $U(t)$ and $F_t^F(t)$ from (57) and (58), the following expression can be obtained

$$\begin{aligned}\dot{V} \leq\ & -k_{p1}\|\bar{x}_h\|^2 - k_{r1}\|r\|^2 - k_\eta\|\eta\|^2 \\ & + \left(\|r\|\zeta_1 - \frac{\|r\|^2\zeta_1^2}{\varepsilon_1}\right) + \left(\|\eta\|\zeta_2 - \frac{\|\eta\|^2\zeta_2^2}{\varepsilon_2}\right) \\ & + \left(\|\bar{x}_h\|\,|\beta_1| - k_{p2}\|\bar{x}_h\|^2\right) \\ & + \left(\|r\|\,|\beta_2| - k_{r2}\|r\|^2\right)\end{aligned} \tag{62}$$

where, based on Assumption 4, $\beta_1, \beta_2 \in \mathbb{R}^1$ are two positive, bounding constants chosen such that

$$\beta_1 \geq \left\|R_F^C\delta\right\| + \left\|S\left(\omega_{IL}^C\right)\bar{R}x_{CL^*}^C\right\| + \left\|v_{IL}^C\right\|, \tag{63}$$
$$\beta_2 \geq \|N_{12}\| \tag{64}$$

and $k_{p1}, k_{r1}, k_{p2}, k_{r2} \in \mathbb{R}^1$ are positive, scalar constants such that $k_p = k_{p1} + k_{p2}$ and $k_r = k_{r1} + k_{r2}$. After applying the non-linear damping argument from [12], the bracketed terms in the above expression can be upper-bounded as follows

$$\begin{aligned}\|r\|\zeta_1\left(1 - \frac{\|r\|\zeta_1}{\varepsilon_1}\right) &\leq \varepsilon_1, \\ \|\eta\|\zeta_2\left(1 - \frac{\|\eta\|\zeta_2}{\varepsilon_2}\right) &\leq \varepsilon_2, \\ \|\bar{x}_h\|\left(|\beta_1| - k_{p2}\|\bar{x}_h\|\right) &\leq \tfrac{|\beta_1|}{k_{p2}}, \\ \|r\|\left(|\beta_2| - k_{r2}\|r\|\right) &\leq \tfrac{|\beta_2|}{k_{r2}}.\end{aligned} \tag{65}$$

From (62) and (65), $\dot{V}(t)$ can be upper bounded in the following manner

$$\dot{V} \leq -k_{p1}\|\bar{x}_h\|^2 - k_{r1}\|r\|^2 - k_\eta\|\eta\|^2 + \varepsilon \tag{66}$$

where $\varepsilon \triangleq \varepsilon_1 + \varepsilon_2 + \frac{|\beta_1|}{k_{p2}} + \frac{|\beta_2|}{k_{r2}} \in \mathbb{R}^1$. The solution to the above differential equation allows us to upper-bound the tracking errors in the following manner

$$\|\bar{x}_h(t)\|, \|e_\theta(t)\| \leq V(t) \leq \alpha_1 \exp\left(-\alpha_2 t\right) + \alpha_3 \tag{67}$$

where $\alpha_1 = V(0)$, $\alpha_2 = \dfrac{\min\left(k_{p1}, k_{r1}, k_n\right)}{\max\left(\frac{1}{2}, d^*, \lambda_{\max}\left(M\right)\right)}$, and $\alpha_3 = \dfrac{\varepsilon}{\alpha_2}$ are positive scalar constants, and $\lambda_{\max}(M) \in \mathbb{R}^1$ denotes the largest eigenvalue of the inertia matrix of the follower UAV.

From (61) and (66), it can be seen that $\bar{x}_h(t), r(t), \eta(t) \in \mathcal{L}_\infty$. From (35) and (36), it follows that $v_{IF}^F(t), e_\theta(t) \in \mathcal{L}_\infty$, and consequently, from the UAV translational dynamics in (1), $\dot{x}_{IF}^F(t) \in \mathcal{L}_\infty$. Since $\bar{x}_h(t)$ is bounded, from (15) and Figure 2, it can be seen that $x_{IF}^I(t) \in \mathcal{L}_\infty$. From (39), $N_{11}(\cdot) \in \mathcal{L}_\infty$, and hence, from (54), $\zeta_1(\cdot) \in \mathcal{L}_\infty$. It follows from (57) and (54) that $U(t) \in \mathcal{L}_\infty$. Consequently, it is easy to show that $\bar{U}_n(t), \bar{U}(t) \in \mathcal{L}_\infty$ from (50) and (48), respectively; therefore, $\omega_n(t), \omega_{IF}^F(t), \dot{\theta}_c(t), u_1(t) \in \mathcal{L}_\infty$. The PTCU Jacobian $J_c(t)$ is a bounded function of pan/tilt angles $\theta_c(t)$ and hence, from (9) it can be inferred that $\omega_{FC}^F(t) \in \mathcal{L}_\infty$, which leads us to the observation that $\omega_{IC}^I(t) \in \mathcal{L}_\infty$. We have now demonstrated that every term in the expressions for the time derivatives of $r(t)$, $\bar{x}_h(t)$ and $e_\theta(t)$, as shown in (45), (37) and (25), are bounded. As a result, $\dot{U}(t), \dot{\bar{U}}_n(t) \in \mathcal{L}_\infty$ (see (57)), and the

follower translational acceleration $\dot{v}_{IF}^{F}(t) \in \mathcal{L}_\infty$ (as revealed by taking the time derivative of $r_p(t)$ in (36)). Hence, from (53) and (55), $N_{22}(\cdot), \zeta_2(\cdot) \in \mathcal{L}_\infty$. From the preceding signal chase, and from (58), we can conclude that $F_t^F(t) \in \mathcal{L}_\infty$, and hence, from (4), $\dot{\omega}_{IF}^{F}(t) \in \mathcal{L}_\infty$. Therefore, all signals remain bounded during closed loop operation. ■

Remark 8: The control objective is formulated as the desire to control the follower UAV such that the images obtained from the PTCU and a reference image of the features on the leader vehicle coincide. Since the origins of the follower UAV frame and the camera frame coincide, it can be seen from (20) and (67) that the controller developed in Section IV will maintain the follower at a fixed position behind the leader. However, the orientation objective in (20) is formulated as the desire to control the PTCU orientation $R_L^C(t)$ relative to the leader, and hence, we cannot state how the orientation of the UAV ($R_F^I(t)$) will evolve with time.

V. Simulation Results

The following UAV parameters were used for simulation of the follower control algorithm

$$m = 0.6 \text{ (kg)}, \tag{68}$$

$$M = \begin{bmatrix} 0.4 & 0 & 0 \\ 0 & 0.4 & 0 \\ 0 & 0 & 0.6 \end{bmatrix} \text{ (kg-m}^2\text{)}. \tag{69}$$

The simulated leader vehicle is a mobile robot moving in a circular trajectory on the ground plane (XY). The perspective camera on the follower was simulated to track eight coplanar feature points that formed the corners of two concentric squares on top of the leader vehicle. In a practical implementation, a real-time implementation of an automatic feature tracking algorithm such as the Lucas-Kanade tracker [13] could be utilized to track features on the leader. The homography matrix was computed from the image coordinates of the features relative to the camera frame using the least-squares technique. An implementation of the algorithm given in [4] was utilized to decompose the homography matrix in order to compute the error signals given in (23) and (30). The initial position of the UAV was set to 5 meters above the leader vehicle (*i.e.*, $z = -5$ m), and the desired time varying position of the follower UAV was selected to be 10 meters above the leader vehicle. The initial and desired orientation of the UAV were $\begin{bmatrix} 0.01 & 0.01 & 1.57 \end{bmatrix}^T$ radians and $\begin{bmatrix} 0 & 0 & 0 \end{bmatrix}^T$ radians, respectively. The trajectories of the leader and follower vehicles are shown in Figure 3, while the time evolution of position and orientation error signals are shown in Figure 4. The UAV control effort and the PTCU angular velocity input remains bounded within reasonable values, as shown in Figures 5 and 6 respectively. For a realistic simulation, the UAV thrust force $u_1(t)$ was saturated at 20 N and torques $u_2(t)$ to $u_4(t)$ were saturated at 5 N-m to restrict initial spikes in the control signal. The following control gains were used, selected based on trial and error

$$k_p = 20,\ k_r = 10,\ k_\eta = 100, \tag{70}$$

$$\varepsilon_1 = 1,\ \varepsilon_2 = 0.1, \tag{71}$$

$$\delta = \begin{bmatrix} 0.1 & 0 & 0.5 \end{bmatrix}^T. \tag{72}$$

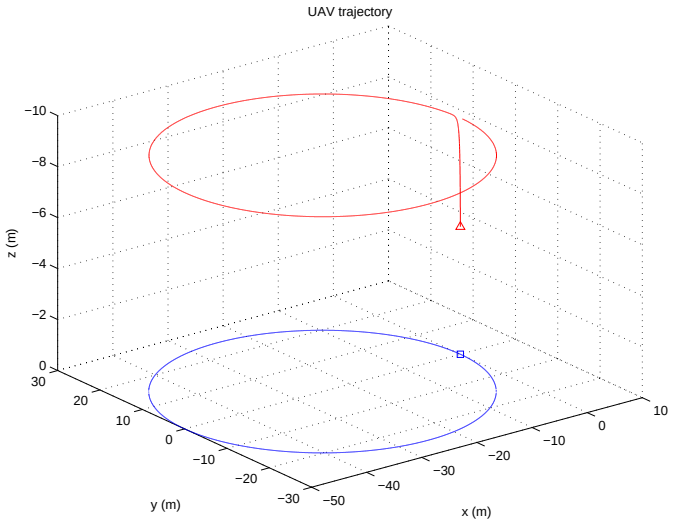

Fig. 3. The leader (□) and follower (△) trajectories.

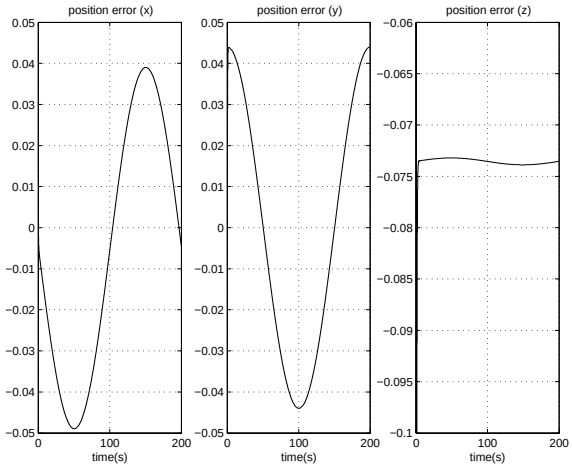

Fig. 4. Follower position errors ($\bar{x}_h(t)$, dimensionless). Orientation errors ($e_\theta(t)$, m-rad.

The nonlinearities $N_1(\cdot)$ and $N_2(\cdot)$ in (2) and (4) were assumed to be of the following form

$$N_1 = -0.5\text{Tanh}(v_{IF}^F) \tag{73}$$

$$N_2 = -0.5\text{Tanh}(\omega_{IF}^F) \tag{74}$$

where $\text{Tanh}(v) \in \mathbb{R}^n$ is a vector whose elements are defined as the hyperbolic tangent of elements of the vector $v(t) \in \mathbb{R}^n$. The scalar functions $\zeta_1(\cdot)$ and $\zeta_2(\cdot)$ in (54) and (55), respectively, were selected as follows

$$\zeta_1 = 0.1 \left\| v_{IF}^F \right\|_s, \tag{75}$$

$$\zeta_2 = 0.1 \left\| v_{IF}^F \right\| + 0.1 \left\| \omega_{IF}^F \right\|. \tag{76}$$

VI. Conclusions

This paper presented the design of a vision-based controller for an underactuated UAV equipped with a pan-tilt camera to achieve the objective of following a leader vehicle

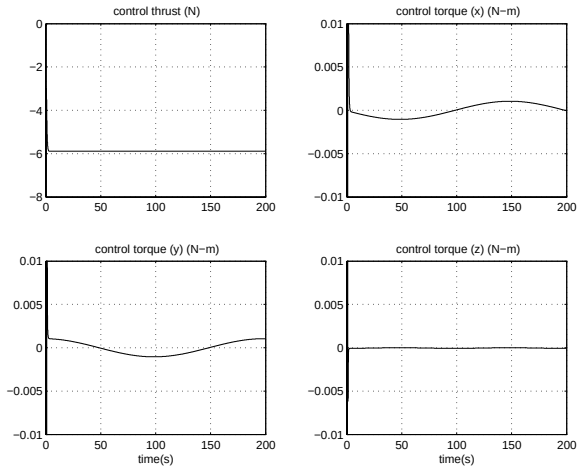

Fig. 5. Time evolution of control effort for the follower UAV.

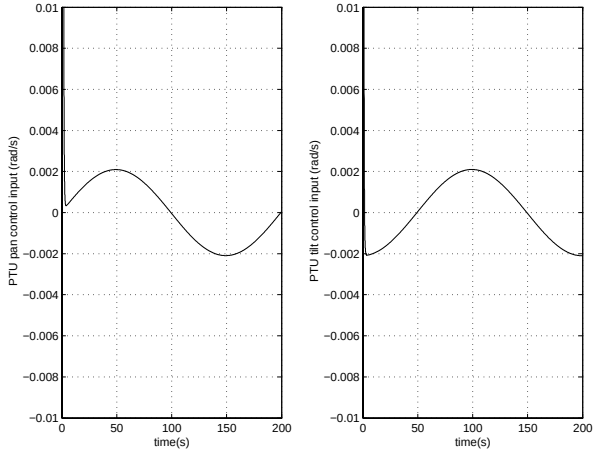

Fig. 6. The PTCU angular velocity inputs on the follower UAV.

autonomously. The development of the relative position and orientation error signals employed homography-based techniques, and the controller design was developed using the backstepping approach. The proposed controller was shown to achieve uniform ultimate bounded (UUB) tracking. Six control inputs ($u_1(t)$ to $u_4(t)$ and $\dot{\theta}_c(t)$) were utilized to control the six d.o.f combined UAV-PTCU system to achieve the objective of matching the images captured by the camera with a reference image of the leader. This would not be possible without the two additional d.o.f. provided by the PTCU to compensate for the two rotational d.o.f. in the UAV lost towards achieving the position control objective. It should be noted that if the PTCU is removed, we can follow the approach outlined in our previous work [7] to design a controller that achieves 3 d.o.f position tracking and yaw (rotation about UAV vertical axis) tracking.

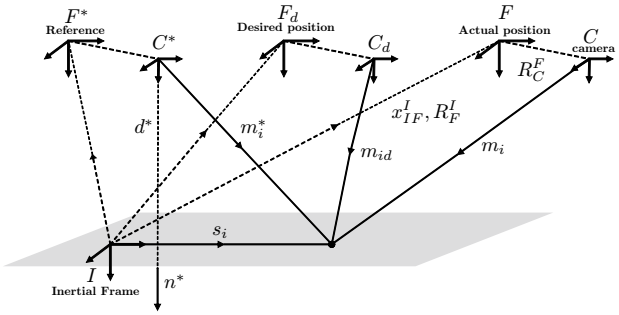

Fig. 7. Geometrical relationships for vision-based trajectory tracking.

APPENDIX I
EXTENSION TO VISION-BASED TRAJECTORY TRACKING

With a few modifications in geometric modeling, the leader-follower strategy described in the paper can be adapted to a vision-based trajectory tracking strategy, where the desired trajectory of the UAV is defined in terms of a sequence of images of stationary features on the ground, captured, for example, during a previous flight of the UAV. Along this line of reasoning, we follow an approach similar to that presented in [6]. At every instant of time, the image captured from the UAV in flight, and a corresponding image from the previously obtained desired video sequence are compared to a reference image of the ground features in order to compute the relative position and orientation tracking errors. The geometrical relationships between the various coordinate frames are shown in Figure 7. As before, the origin of the camera frame is assumed to coincide with the UAV frame, and they are shown separate from each other in Figure 7 for the sake of clarity. The optical axis of the PTCU is pointed downwards by default, along the z axis of the camera frame and the UAV. The PTCU kinematics are given in expressions (8) to (10). Let the constant vector $s_i \in \mathbb{R}^3$ expressed in the inertial frame I define the coordinates of the i^{th} visual feature on the ground, and let $m_i(t) \in \mathbb{R}^3$ denote the Euclidean coordinates of the same feature defined in the UAV's camera frame C. The objective is to control the UAV, denoted by coordinate frame F, such that the images of the visual features on the ground obtained from the camera on the UAV (denoted by C), coincide with the images of the same visual features captured by the camera when the UAV is at the desired location, denoted by the coordinate frame F_d shown in Figure 7. Let $m_{id}(t) \in \mathbb{R}^3$ denote the 3D Euclidean coordinates of the i^{th} visual feature as seen by the camera on the UAV at the desired position, and let $m_i^* \in \mathbb{R}^3$denote the constant Euclidean coordinates of the same feature point relative to the camera frame when the UAV is at its reference position F^*. Based on the geometry in Figure 7, the Euclidean coordinates of the same visual feature, as seen by the on-board camera from the three camera locations denoted by C, C_d and C^* are related as follows

$$\begin{aligned} m_i &= \bar{x} + \bar{R} m_i^* \\ m_{id} &= \bar{x}_d + \bar{R}_d m_i^* \end{aligned} \tag{77}$$

where the new position and orientation variables are defined in the following manner

$$\bar{R} \;=\; R_F^C R_I^F R_{F^*}^I R_{C^*}^{F^*}, \tag{78}$$

$$\bar{R}_d = R_{F_d}^{C_d} R_I^{F_d} R_{F^*}^I R_{C^*}^{F^*}, \quad (79)$$

$$\bar{x} = R_F^C R_I^F \left(x_{IF^*}^I - x_{IF}^I \right), \quad (80)$$

$$\bar{x}_d = R_{F_d}^{C_d} R_I^{F_d} \left(x_{IF^*}^I - x_{IF_d}^I \right). \quad (81)$$

After defining the relationship between the normalized Euclidean coordinates and the 2D homogeneous image coordinates of the visual features as shown in (18), the relationships in (77) can be expressed in terms of their image coordinates as follows

$$\begin{aligned} p_i &= \alpha_i A \left(\bar{R} + \frac{1}{d^*} \bar{x} n^{*T} \right) A^{-1} p_i^*, \\ p_{id} &= \alpha_{id} A \left(\bar{R}_d + \frac{1}{d^*} \bar{x}_d n^{*T} \right) A^{-1} p_i^* \end{aligned} \quad (82)$$

where $\alpha_{id}(t) = \frac{z_i^*}{z_{id}(t)}$, $p_{id}(t) = A\frac{m_{id}(t)}{z_{id}(t)} \in \mathbb{R}^1$, $n^* \in \mathbb{R}^3$ denotes the normal vector to the ground plane defined in the frame C^*, and $d^* \in \mathbb{R}^1$ is the distance to the ground plane from the frame C^*. If four or more visual features on the ground can be continuously tracked by the on-board vision system on the UAV, the homography matrices shown in brackets in (82) can be computed, which can be subsequently decomposed utilizing the algorithms previously mentioned in order to calculate the rotation matrices $\bar{R}(t)$ and $\bar{R}_d(t)$, and the scaled translation vectors $\frac{\bar{x}(t)}{d^*}$ and $\frac{\bar{x}_d(t)}{d^*}$.

Control Formulation: In addition to Assumptions 1 to 4 stated for the leader-follower case, we utilize the following additional assumptions in the control development

Assumption 8: The scaled position and orientation variables $\bar{R}(t), \bar{R}_d(t), \frac{1}{d^*}\bar{x}(t)$ and $\frac{1}{d^*}\bar{x}_d(t)$ are available from the vision system.

Assumption 9: The desired position and velocity signals are bounded, *i.e.*, $x_{IF_d}^I(t), v_{IF_d}^I(t), \omega_{IF_d}^I(t) \in \mathcal{L}_\infty$.

Assumption 10: All the visual features tracked by the vision system are always within the field of view of the camera, and are in front of the camera (*i.e.*, $z_i > \gamma$ for every feature point, where $\gamma \in \mathbb{R}^1$, is a positive scalar constant).

The position error signal, denoted by $e_p(t) \in \mathbb{R}^3$, is defined in the following manner

$$e_p \triangleq \frac{1}{d^*} R_I^F \left(x_{IF}^I - x_{IF_d}^I \right). \quad (83)$$

After some mathematical manipulation, it can be shown that the position error signal defined in (83) can be written in terms of measurable signals from the vision system as follows

$$e_p = R_C^F R_e \bar{x}_{dh} - R_C^F \bar{x}_h \quad (84)$$

where

$$R_e = \bar{R} \bar{R}_d^T, \quad (85)$$

$$\bar{x}_{dh} = \frac{1}{d^*} \bar{x}_d, \quad (86)$$

$$\bar{x}_h = \frac{1}{d^*} \bar{x}. \quad (87)$$

Analogous to the leader-follower case, the objective of orientation tracking is achieved if $R_e(t) \to I_{3\times 3}$ as $t \to \infty$; hence, the orientation error signal, denoted by $e_\theta(t) \in \mathbb{R}^3$, is defined in terms of the axis-angle representation of the rotation matrix $R_e(t)$ as follows

$$e_\theta \triangleq \mu \phi \quad (88)$$

where

$$\phi = \cos^{-1}\left(\frac{1}{2} \left(\text{tr}(R_e) - 1 \right) \right), \quad S(\mu) = \frac{R_e - R_e^T}{2\sin(\phi)}. \quad (89)$$

After taking the time derivative of the error signals in (83) and (88), the following open-loop error dynamics are obtained

$$d^* \dot{e}_p = v_{IF}^F - S\left(\omega_{IF}^F\right) d^* e_p - R_I^F \dot{x}_{IF_d}^I \quad (90)$$

$$\begin{aligned} \dot{e}_\theta &= -L_\omega \omega_{C_d C}^C \\ &= -L_\omega R_F^C \omega_{IF}^F - L_\omega R_F^C J_c \dot{\theta}_c + L_\omega \omega_{IC_d}^C. \end{aligned} \quad (91)$$

Based on the subsequent Lyapunov analysis, an auxiliary signal $r(t) \in \mathbb{R}^6$ is defined as follows

$$r \triangleq \begin{bmatrix} r_p^T & e_\theta^T \end{bmatrix}^T \quad (92)$$

where $r_p(t) \in \mathbb{R}^3$ is defined in the following manner

$$r_p \triangleq k_p e_p + v_{IF}^F + \delta \quad (93)$$

and the constants $k_p \in \mathbb{R}^1$ and $\delta \in \mathbb{R}^3$ have the same definitions as in the leader-follower case. After substituting for $v_{IF}^F(t)$ from (93) in (83), the following alternate expression for the open-loop position error dynamics can be obtained

$$\begin{aligned} d^* \dot{e}_p &= r_p - k_p e_p - \delta - S\left(\omega_{IF}^F\right) d^* e_p \\ &\quad - R_I^F \dot{x}_{IF_d}^I. \end{aligned} \quad (94)$$

The time derivative of (92) is complex, but it can be shown that, after substituting (90) for $\dot{e}_p(t)$, the dynamics in (2) for $\dot{v}_{IF}^F(t)$, (10) for $\dot{R}_F^C(t)$, and (91) for $\dot{e}_\theta(t)$, the following simplified expression for the open loop dynamics of $r(t)$ can be developed

$$\dot{r} = \begin{bmatrix} -S\left(\omega_{IF}^F\right) r_p \\ 0_{3\times 1} \end{bmatrix} + \bar{B}\bar{U} + N_{11} + N_{12} \quad (95)$$

where

$$\bar{B} = B_1 B_2, \quad (96)$$

$$B_1 = \begin{bmatrix} I_{3\times 3} & 0_{3\times 3} \\ 0_{3\times 3} & -L_\omega R_F^C \end{bmatrix}, \quad (97)$$

$$B_2 = \begin{bmatrix} 0 & 0 & -\delta_3 & \delta_2 & 0 & 0 \\ 0 & \delta_3 & 0 & -\delta_1 & 0 & 0 \\ \frac{1}{m} & -\delta_2 & \delta_1 & 0 & 0 & 0 \\ 0 & 1 & 0 & 0 & 1 & 0 \\ 0 & 0 & 1 & 0 & 0 & \text{c}(\theta_p) \\ 0 & 0 & 0 & 1 & 0 & \text{s}(\theta_p) \end{bmatrix}, \quad (98)$$

$$\bar{U} = \begin{bmatrix} u_1 \\ \omega_{IF}^F \\ \dot{\theta}_c \end{bmatrix}, \quad (99)$$

$$N_{11} \triangleq \begin{bmatrix} \frac{k_p}{d^*} v_{IF}^F + \frac{1}{m} N_1 \\ 0_{3\times 1} \end{bmatrix}, \quad (100)$$

$$N_{12} \triangleq \begin{bmatrix} -\frac{k_p}{d^*} R_I^F \dot{x}_{IF_d}^I \\ L_\omega \omega_{IC_d}^C \end{bmatrix}. \quad (101)$$

Remark 9: After utilizing Assumption 4, it can be shown that $B_2(t) \in \mathbb{R}^{6\times 6}$ is full-ranked if $\delta_3 \neq 0$. Since it can be easily verified that $B_1(t) \in \mathbb{R}^{6\times 6}$ is invertible, it follows from (96) that $\bar{B}(t)$ is invertible.

Remark 10: Note that the dynamics for $e_\theta(t)$, $e_p(t)$ and $r(t)$, as given by the expressions in (91), (94) and (95),

respectively, are similar in form to the dynamics of the error systems for the leader-follower case, given by (25), (37) and (45). Hence, we follow the same approach as the leader-follower problem in the subsequent control design.

Control Design: After defining the desired control signal $\bar{U}_n(t)$ and the backstepping error signal $\eta(t)$, and subsequently designing the desired control signal $\bar{U}_n(t)$ as shown in (46), (47), and (50), respectively, the dynamics of $r(t)$ can be expressed as follows

$$\dot{r} = \begin{bmatrix} -S\left(\omega_{IF}^F\right) r_p \\ 0_{3\times 1} \end{bmatrix} + U - \bar{B}\Pi^T \eta + N_{11} + N_{12}. \quad (102)$$

The dynamics for $\eta(t)$ is the same as before, and given by the expression in (52). Based on the stability analysis provided in the next sub-section, the control inputs are designed in the following manner

$$U = -k_r r - \begin{bmatrix} e_p \\ 0_{3\times 1} \end{bmatrix} - r\frac{\zeta_1^2}{\varepsilon_1}, \quad (103)$$

$$F_t^F = M\Pi\dot{\bar{U}}_{n1} + S\left(\omega_{IF}^F\right) M\omega_{IF}^F + k_\eta \eta - \Pi\bar{B}^T r + \eta\frac{\zeta_2^2}{\varepsilon_2} \quad (104)$$

where $k_r, k_\eta \in \mathbb{R}^1$ are positive, scalar control gains, $\varepsilon_1, \varepsilon_2 \in \mathbb{R}^1$ are positive, scalar constants, and $\zeta_1(\cdot), \zeta_2(\cdot) \in \mathbb{R}^1$ are known positive, scalar, non-decreasing bounding functions on $N_{11}(\cdot)$ and $N_{22}(\cdot)$, constructed like (54) and (55), respectively. $\dot{\bar{U}}_{n1}(t)$, $\dot{\bar{U}}_{n2}(t) \in \mathbb{R}^6$ are the known and unknown terms, respectively, in the time derivative of $\bar{U}_n(t)$, and their expressions are given in Appendix II.

Theorem 2: Given the error dynamics of (94), (102) and (52), the translational force input and the rotational torque input developed in (103) and (104), respectively, guarantees uniform ultimate boundededness (UUB) in the position error signal $e_p(t)$ and the orientation error signal $e_\theta(t)$ in a neighborhood about zero in the sense that

$$\|e_p(t)\|, \|e_\theta(t)\| \leq \alpha_1 \exp\left(-\alpha_2 t\right) + \alpha_3 \quad (105)$$

where $\alpha_1, \alpha_2, \alpha_3 \in \mathbb{R}^1$ are adjustable, positive constants.

Proof: We choose the following non-negative scalar function as the Lyapunov candidate to prove the above theorem

$$V \triangleq \frac{1}{2} d^* e_p^T e_p + \frac{1}{2} r^T r + \frac{1}{2} \eta^T M \eta. \quad (106)$$

After taking the time derivative of (106), substituting the dynamics for $\dot{e}_p(t), \dot{r}(t)$ and $\dot{\eta}(t)$ from (94), (102) and (52), and substituting the expressions for $U(t)$ and $F_t^F(t)$ from (103) and (104), the following expression can be obtained

$$\dot{V} \leq -k_{p1}\|e_p\|^2 - k_{r1}\|r\|^2 - k_\eta\|\eta\|^2 + \left(\|r\|\zeta_1 - \frac{\|r\|^2\zeta_1^2}{\varepsilon_1}\right) + \left(\|\eta\|\zeta_2 - \frac{\|\eta\|^2\zeta_2^2}{\varepsilon_2}\right) + \left(\|e_p\|\left|\beta_1\right| - k_{p2}\|e_p\|^2\right) + \left(\|r\|\left|\beta_2\right| - k_{r2}\|r\|^2\right) \quad (107)$$

where, based on Assumption 5, $\beta_1, \beta_2 \in \mathbb{R}^1$ are two positive, bounding constants chosen such that

$$\beta_1 \geq \|\delta\| + \left\|R_I^F \dot{x}_{IFd}^I\right\|, \quad (108)$$

$$\beta_2 \geq \|N_{12}\| \quad (109)$$

and $k_{p1}, k_{r1}, k_{p2}, k_{r2} \in \mathbb{R}^1$ are positive, scalar constants such that $k_p = k_{p1} + k_{p2}$ and $k_r = k_{r1} + k_{r2}$. After applying the non-linear damping argument from [12], the bracketed terms in the above expression can be upper-bounded as follows

$$\begin{aligned} \|r\|\zeta_1\left(1 - \frac{\|r\|\zeta_1}{\varepsilon_1}\right) &\leq \varepsilon_1, \\ \|\eta\|\zeta_2\left(1 - \frac{\|\eta\|\zeta_2}{\varepsilon_2}\right) &\leq \varepsilon_2, \\ \|e_p\|\left(\left|\beta_1\right| - k_{p2}\|e_p\|\right) &\leq \frac{|\beta_1|}{k_{p2}}, \\ \|r\|\left(\left|\beta_2\right| - k_{r2}\|r\|\right) &\leq \frac{|\beta_2|}{k_{r2}}. \end{aligned} \quad (110)$$

From (107) and (110), $\dot{V}(t)$ can be upper bounded in the following manner

$$\dot{V} \leq -k_{p1}\|e_p\|^2 - k_{r1}\|r\|^2 - k_\eta\|\eta\|^2 + \varepsilon \quad (111)$$

where $\varepsilon \triangleq \varepsilon_1 + \varepsilon_2 + \frac{|\beta_1|}{k_{p2}} + \frac{|\beta_2|}{k_{r2}} \in \mathbb{R}^1$. The solution to the above differential equation allows us to upper-bound the tracking errors in the following manner

$$\|e_p(t)\|, \|e_\theta(t)\| \leq V(t) \leq \alpha_1 \exp\left(-\alpha_2 t\right) + \alpha_3 \quad (112)$$

where $\alpha_1 = V(0)$, $\alpha_2 = \dfrac{\min\left(k_{p1}, k_{r1}, k_n\right)}{\max\left(\dfrac{1}{2}, d^*, \lambda_{\max}\left(M\right)\right)}$, and $\alpha_3 = \dfrac{\varepsilon}{\alpha_2}$ are positive scalar constants, and $\lambda_{\max}(M) \in \mathbb{R}^1$ denotes the largest eigenvalue of the inertia matrix of the UAV.

We now proceed to establish the boundedness of all signals in the system. As evident from (106) and (111), $e_p(t), r(t), e_\theta(t), \eta(t) \in \mathcal{L}_\infty$. From Assumption 5 stated previously, and from (83), (88), (92), and (93), it follows that $x_{IF}^I(t), e_\theta(t), v_{IF}^F(t) \in \mathcal{L}_\infty$, and from (101), $N_{12}(t) \in \mathcal{L}_\infty$. It can be observed from (1) that $\dot{x}_{IF}^I(t) \in \mathcal{L}_\infty$. From (100), $N_{11}(\cdot) \in \mathcal{L}_\infty$, and hence, from(54), $\zeta_1(\cdot) \in \mathcal{L}_\infty$. Therefore, $U(t) \in \mathcal{L}_\infty$ (see (103)), and consequently, $\bar{U}_n(t)$ and $\bar{U}(t)$ are all bounded signals. Hence, it is evident from (46) and (99) that $\omega_n(t), \omega_{IF}^F(t) \in \mathcal{L}_\infty$, and $u_1(t), \dot{\theta}_c(t) \in \mathcal{L}_\infty$. We have now shown that all signals that define the time derivatives of $r(t), e_p(t)$ and $e_\theta(t)$ are bounded. Hence, it is easy to see from an examination of the time derivatives of (93) and (103) that $\dot{v}_{IF}^F(t), \dot{U}(t) \in \mathcal{L}_\infty$. Hence, $\dot{\bar{U}}_n(t) \in \mathcal{L}_\infty$. The dynamics of $\eta(t)$ is the same as in the leader-follower case, and it is evident that $N_{22}(\cdot) \in \mathcal{L}_\infty$. Hence, it follows from (55) that $\zeta_2(\cdot) \in \mathcal{L}_\infty$. We therefore conclude from (104) that $F_t^F(t) \in \mathcal{L}_\infty$, and from the UAV rotational dynamics in (4) that $\dot{\omega}_{IF}^F(t) \in \mathcal{L}_\infty$. Hence, all signals in the system remain bounded during closed loop operation. ■

Simulation Results: The UAV mass and inertial parameters were selected as given in (68) and (69), respectively. The simulated vision system is similar to that described for the leader-follower case, except that the feature points were assumed static and located on the ground plane. The desired trajectory was a 25 meters radius circular path in the XY plane, 10 meters

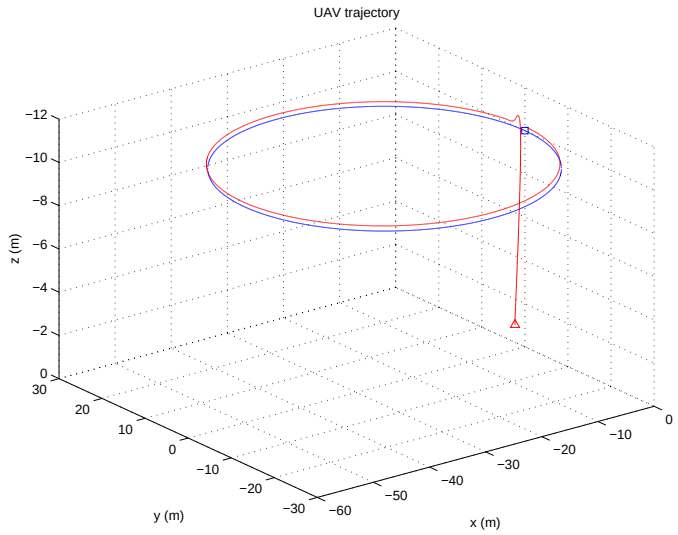

Fig. 8. The desired (□) and actual trajectories (△).

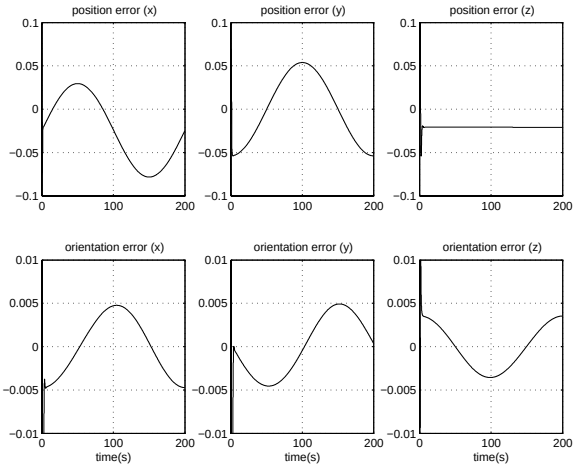

Fig. 9. UAV position ($e_p(t)$, dimensionless) and orientation ($e_\theta(t)$, m-rad.) tracking errors.

above ground ($z = -10$ m). The UAV initial position and orientation angles were set to $\begin{bmatrix} -1 & 1 & -1 \end{bmatrix}^T$ (meters) and $\begin{bmatrix} 0.01 & 0.01 & 1.57 \end{bmatrix}^T$ (radians), respectively. Through trial and error, the various control gains were selected as follows

$$k_p = 20,\ k_r = 2,\ k_\eta = 20 \quad (113)$$

$$\varepsilon_1 = 1,\ \varepsilon_2 = 0.1 \quad (114)$$

$$\delta = \begin{bmatrix} 0.5 & 0 & 0.5 \end{bmatrix}^T. \quad (115)$$

The desired and the actual trajectories are depicted in Figure 8. The error signals $e_p(t)$ and $e_\theta(t)$ are shown in Figure 9. From Figure 10, it can be seen that the control inputs to the UAV remain bounded at all times. Similarly, the PTCU angular velocity input is shown in Figure 11.

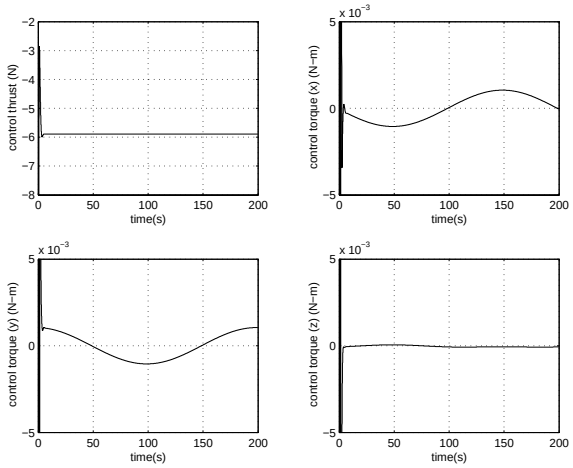

Fig. 10. Control effort for the trajectory tracking UAV.

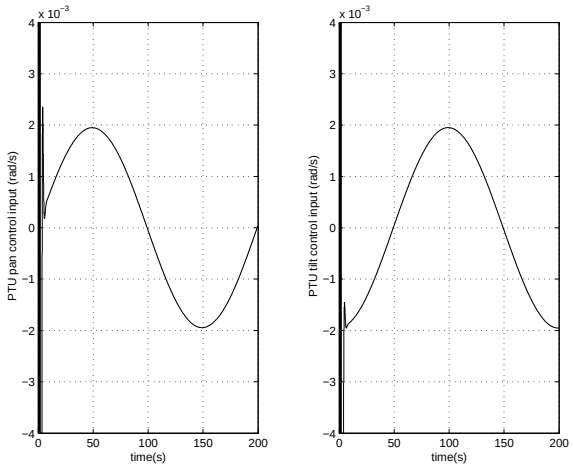

Fig. 11. PTCU angular velocity inputs.

APPENDIX II
TIME DERIVATIVE OF AUXILIARY CONTROL SIGNAL $\bar{U}_n(t)$

From (50), the auxiliary control signal $\bar{U}_n(t)$ is given as follows

$$\bar{U}_n = B_2^{-1} B_1^{-1} U \quad (116)$$

and the known and unknown components in its time derivative can be written as follows

$$\dot{\bar{U}}_{n1} = B_2^{-1} B_1^{-1} \dot{U}_1 + B_2^{-1} \dot{B}_{11}^{-1} U + \dot{B}_2^{-1} B_1^{-1} U, \quad (117)$$

$$\dot{\bar{U}}_{n2} = B_2^{-1} B_1^{-1} \dot{U}_2 + B_2^{-1} \dot{B}_{12}^{-1} U \quad (118)$$

where $\dot{B}_{11}^{-1}(t)$ and $\dot{U}_1(t)$ denote the known terms in the time derivatives of $B_1^{-1}(t)$ and $U(t)$, respectively, and similarly, $\dot{B}_{12}^{-1}(t)$ and $\dot{U}_2(t)$ denote the unknown terms. We will now show the expressions for each of the terms in the equations (116), (117) and (118) for the leader-follower case presented in the body of the paper, and the trajectory tracking development provided in Appendix I.

Leader-Follower Case: The inverse of $B_1(t)$ and $B_2(t)$ defined in (42) and (43), respectively, can be expressed as

follows

$$B_1^{-1} = \begin{bmatrix} -R_C^F & 0_{3\times3} \\ 0_{3\times3} & -R_C^F L_\omega^{-1} \end{bmatrix}, \quad (119)$$

$$B_2^{-1} = \begin{bmatrix} \frac{m\delta_1}{\delta_3} & \frac{m\delta_2}{\delta_3} & m \\ \frac{-\sin(\theta_p)\delta_1}{\delta_3\alpha_1} & \frac{1}{\delta_3} & 0 \\ \frac{-\cos(\theta_p)}{\alpha_1} & 0 & 0 \\ \frac{-\sin(\theta_p)}{\alpha_1} & 0 & 0 \\ \frac{\sin(\theta_p)\delta_1}{\delta_3\alpha_1} & \frac{-1}{\delta_3} & 0 \\ \frac{1}{\alpha_1} & 0 & 0 \end{bmatrix} \begin{bmatrix} 0 & 0 & 0 \\ 0 & \frac{-\sin(\theta_p)\delta_1}{\alpha_1} & \frac{\cos(\theta_p)\delta_1}{\alpha_1} \\ 0 & \frac{-\sin(\theta_p)\delta_2}{\alpha_1} & \frac{\cos(\theta_p)\delta_2}{\alpha_1} \\ 0 & \frac{-\sin(\theta_p)\delta_3}{\alpha_1} & \frac{\cos(\theta_p)\delta_3}{\alpha_1} \\ 1 & \frac{\sin(\theta_p)\delta_1}{\alpha_1} & \frac{-\cos(\theta_p)\delta_1}{\alpha_1} \\ 0 & \frac{\delta_3}{\alpha_1} & \frac{-\delta_2}{\alpha_1} \end{bmatrix}, \quad (120)$$

$$\alpha_1 = \cos(\theta_p)\delta_3 - \sin(\theta_p)\delta_2 \quad (121)$$

where

$$L_\omega^{-1} = I_{3\times3} + \tfrac{\phi}{2}\,\mathrm{sinc}^2\left(\tfrac{\phi}{2}\right) S(\mu) + (1-\,\mathrm{sinc}(\phi))\, S(\mu)^2. \quad (122)$$

The time derivatives of $B_1^{-1}(t)$ and $B_2^{-1}(t)$ are as follows

$$\dot{B}_{11}^{-1} = \begin{bmatrix} -\dot{R}_C^F & 0_{3\times3} \\ 0_{3\times3} & -R_C^F\dot{L}_{\omega 1}^{-1} - \dot{R}_C^F L_\omega^{-1} \end{bmatrix}, \quad (123)$$

$$\dot{B}_{12}^{-1} = \begin{bmatrix} 0_{3\times3} & 0_{3\times3} \\ 0_{3\times3} & -R_C^F\dot{L}_{\omega 2}^{-1} \end{bmatrix}, \quad (124)$$

$$\dot{B}_2^{-1} = \begin{bmatrix} 0 & 0 & 0 & 0 \\ \frac{-\delta_1}{\alpha_1^2} & 0 & 0 & 0 \\ \frac{-\delta_2}{\alpha_1^2} & 0 & 0 & 0 \\ \frac{-\delta_3}{\alpha_1^2} & 0 & 0 & 0 \\ \frac{\delta_1}{\alpha_1^2} & 0 & 0 & 0 \\ \frac{-\alpha_2}{\alpha_1^2} & 0 & 0 & 0 \end{bmatrix} \begin{bmatrix} 0 & 0 \\ \frac{-\delta_1\delta_3}{\alpha_1^2} & \frac{\delta_1\delta_2}{\alpha_1^2} \\ \frac{-\delta_2\delta_3}{\alpha_1^2} & \frac{\delta_2^2}{\alpha_1^2} \\ \frac{-\delta_3^2}{\alpha_1^2} & \frac{\delta_2\delta_3}{\alpha_1^2} \\ \frac{\delta_1\delta_3}{\alpha_1^2} & \frac{-\delta_1\delta_2}{\alpha_1^2} \\ \frac{-\delta_3\alpha_2}{\alpha_1^2} & \frac{\delta_2\alpha_2}{\alpha_1^2} \end{bmatrix} \dot{\theta}_p, \quad (125)$$

$$\alpha_2 = -\sin(\theta_p)\delta_3 - \cos(\theta_p)\delta_2 \quad (126)$$

where $\dot{R}_C^F(t)$ is given by (10), and the time derivative of $L_\omega^{-1}(t)$ is expressed as the sum of known terms $\dot{L}_{\omega 1}^{-1}(t)$ and unknown terms $\dot{L}_{\omega 2}^{-1}(t)$ as follows

$$\begin{aligned} \dot{L}_{\omega i}^{-1} = {} & S(\mu\mu^T\dot{e}_{\theta i})\left[\left(\,\mathrm{sinc}(\phi) - \tfrac{1}{2}\,\mathrm{sinc}^2\left(\tfrac{\phi}{2}\right)\right) I_{3\times3} \right. \\ & \left. - \left(\frac{\cos(\phi) - \,\mathrm{sinc}(\phi)}{\phi}\right) S(\mu)\right] \\ & - \tfrac{1}{2}\,\mathrm{sinc}^2\left(\tfrac{\phi}{2}\right) S\left(S(\mu)^2\dot{e}_{\theta i}\right) \\ & - \frac{(1-\,\mathrm{sinc}(\phi))}{\phi}\left(\mu\dot{e}_{\theta i}^T S(\mu)^2\right. \\ & \left. + S(\mu)^2\dot{e}_{\theta i}\mu^T\right), \end{aligned} \quad (127)$$

$$\text{where } \dot{e}_{\theta 1} = -L_\omega R_F^C\left(\omega_{IF}^F + J_c\dot{\theta}_c\right), \quad (128)$$

$$\text{and } \dot{e}_{\theta 2} = L_\omega\omega_{IL}^C. \quad (129)$$

Similarly the time derivative for the control signal $U(t)$ defined in (57) can be obtained by substituting the time derivatives for $\bar{x}_h(t)$ and $r(t)$ from (34) and (45), and expressing them in terms of known and unknown terms $\dot{U}_1(t)$ and $\dot{U}_2(t)$, respectively, as follows

$$\begin{aligned} \dot{U}_1 = {} & \left(k_r + \frac{\zeta_1^2}{\varepsilon_1}\right)\left(\begin{bmatrix} S\left(\omega_{IC}^C\right) r_p \\ 0_{3\times1} \end{bmatrix} - \bar{B}\bar{U}\right) \\ & + \begin{bmatrix} S\left(\omega_{IC}^C\right)\bar{x}_h \\ 0_{3\times1} \end{bmatrix} - \frac{2\zeta_1}{\varepsilon_1}\dot{\zeta}_{11} r \end{aligned} \quad (130)$$

$$\begin{aligned} \dot{U}_2 = {} & \frac{1}{d^*}\left(R_F^C v_{IF}^F + S\left(\omega_{IL}^C\right)\bar{R}x_{CL^*}^C - v_{IL}^C\right) \\ & - \left(k_r + \frac{\zeta_1^2}{\varepsilon_1}\right)(N_{11} + N_{12}) - \frac{2\zeta_1}{\varepsilon_1}\dot{\zeta}_{12} r \end{aligned} \quad (131)$$

where $\dot{\zeta}_{11}(t)$ and $\dot{\zeta}_{12}(t)$ are the known and unknown terms in the time derivative of $\zeta_1(t)$.

Trajectory Tracking Case: The inverse of $B_1(t)$ defined in (97) can be expressed as follows

$$B_1^{-1} = \begin{bmatrix} I_{3\times3} & 0_{3\times3} \\ 0_{3\times3} & -R_C^F L_\omega^{-1} \end{bmatrix} \quad (132)$$

where $L_\omega^{-1}(t)$ is defined in (122). The time derivative of $B_{11}^{-1}(t)$ is as follows

$$\dot{B}_{11}^{-1} = \begin{bmatrix} 0_{3\times3} & 0_{3\times3} \\ 0_{3\times3} & -R_C^F\dot{L}_{\omega 1}^{-1} - \dot{R}_C^F L_\omega^{-1} \end{bmatrix} \quad (133)$$

where $\dot{R}_C^F(t)$ is given by (10), the time derivative of $L_\omega^{-1}(t)$ is shown in (127), and $\dot{e}_{\theta 1}(t)$ and $\dot{e}_{\theta 2}(t)$ are given as follows

$$\dot{e}_{\theta 1} = -L_\omega R_F^C\left(\omega_{IF}^F + J_c\dot{\theta}_c\right), \quad (134)$$

$$\dot{e}_{\theta 2} = L_\omega\omega_{IC_d}^C. \quad (135)$$

The expression for $B_2^{-1}(t)$ and its time derivative are given in (120) and (125), respectively. Similarly the time derivative for the control signal $U(t)$ defined in (103) can be obtained by substituting the time derivatives for $e_p(t)$ and $r(t)$ from (90) and (95), and expressing them in terms of known and unknown terms $\dot{U}_1(t)$ and $\dot{U}_2(t)$, respectively, as follows

$$\begin{aligned} \dot{U}_1 = {} & \left(k_r + \frac{\zeta_1^2}{\varepsilon_1}\right)\left(\begin{bmatrix} S\left(\omega_{IF}^F\right) r_p \\ 0_{3\times1} \end{bmatrix} - \bar{B}\bar{U}\right) \\ & + \begin{bmatrix} S\left(\omega_{IF}^F\right) e_p \\ 0_{3\times1} \end{bmatrix} - \frac{2\zeta_1}{\varepsilon_1}\dot{\zeta}_{11} r \end{aligned} \quad (136)$$

$$\begin{aligned} \dot{U}_2 = {} & -\frac{1}{d^*}\left(v_{IF}^F - R_I^F\dot{x}_{IF_d}^I\right) \\ & - \left(k_r + \frac{\zeta_1^2}{\varepsilon_1}\right)(N_{11} + N_{12}) - \frac{2\zeta_1}{\varepsilon_1}\dot{\zeta}_{12} r \end{aligned} \quad (137)$$

where $\dot{\zeta}_{11}(t)$ and $\dot{\zeta}_{12}(t)$ are the known and unknown terms in the time derivative of $\zeta_1(t)$.

ACKNOWLEDGMENT

This work was supported in part by two DOC Grants, an ARO Automotive Center Grant, a DOE Contract, a Honda Corporation Grant, and a DARPA Contract.

REFERENCES

[1] A. Aguiar, and J. Hespanha, "Position Tracking of Underactuated Vehicles," *Proc. of the American Control Conference*, pp. 1988-1993, Denver, CO, June 2003.

[2] E. Altuğ, J. P. Ostrowski, and R. Mahony, "Control of a Quadrotor Helicopter Using Visual Feedback," *Proc. of the 2002 IEEE Int. Conf. on Robotics and Automation*, pp. 72-77, May 2002.

[3] E. Altuğ, J. P. Ostrowski, and C. J. Taylor, "Quadrotor Control Using Dual Camera Visual Feedback," *Proc. of the 2002 IEEE Int. Conf. on Robotics and Automation*, Sept. 2003.

[4] O. Faugeras, *Three-Dimensional Computer Vision*, The MIT Press, ISBN: 0262061589, 1993.

[5] T. I. Fossen, *Marine Control Systems: Guidance, Navigation and Control of Ships, Rigs and Underwater Vehicles*, Marine Cybernetics AS (Norway), ISBN:8292356010, 2002.

[6] J. Chen, W. E. Dixon, D. M. Dawson, and M. McIntire, "Homography-based Visual Servo Tracking Control of a Wheeled Mobile Robot," *IEEE Trans. on Robotics and Automation*, Accepted.

[7] V. K. Chitrakaran, D. M. Dawson, J. Chen, and M. Feemster, "Vision Assisted Landing of an Unmanned Aerial Vehicle," *Proc. of the IEEE Conf. on Decision and Control*, pp. 1465-1470, Dec. 2005.

[8] V. K. Chitrakaran, D. M. Dawson, W. E. Dixon, and J. Chen, "Identification of a Moving Object's Velocity with a Fixed Camera," *Automatica*, Vol. 41, No. 3, pp. 553-562, March 2005.

[9] R. Frezza, and C. Altafini, "Autonomous Landing by Computer Vision: An Application of Path Following in SE(3)," *Proc. of the IEEE Conf. on Decision and Control*, pp. 2527-2532, Dec. 2000.

[10] T. Hamel, R. Mahony, R. Lozano, and J. Ostrowski, "Dynamic Modelling and Configuration Stabilization for an X-4 Flyer," *Proc. of the IFAC World Congress*, Barcelona, Spain, July 2002.

[11] S. A. Hutchinson, G. D. Hager, and P. I. Corke, "A Tutorial on Visual Servo Control," *IEEE Trans. on Robotics and Automation*, Vol. 12, No. 5, pp. 651-670, 1996.

[12] M. Krstić, I. Kanellakopoulos, and P. Kokotović, *Nonlinear and Adaptive Control Design*, New York, NY: John Wiley and Sons, 1995.

[13] B. D. Lucas and T. Kanade, "An Iterative Image Registration Technique with an Application to Stereo Vision," *International Joint Conference on Artificial Intelligence*, pp. 674-679, 1981.

[14] Y. Ma, S. Soatto, J. Košecká, and S. Sastry, *An Invitation to 3D Vision*, Springer-Verlag, ISBN: 0387008934, 2003.

[15] R. Mahony, "Image-Based Visual Servo Control of Aerial Robotic Systems Using Linear Image Features," *IEEE Trans. on Robotics*, Vol. 21, No. 2, pp. 227-239, Apr. 2005.

[16] E. Malis, "Contributions à la modèlisation et à la commande en asservissement visuel," *Ph.D. Thesis*, University of Rennes I, IRISA, France, 1998.

[17] E. Malis, and F. Chaumette, "2 1/2 D Visual Servoing with Respect to Unknown Objects Through a New Estimation Scheme of Camera Displacement," *International Journal of Computer Vision*, Vol. 37, No. 1, pp. 79-97, 2000.

[18] P. McKerrow, "Modelling the Draganflyer Four-Rotor Helicopter," *Proc. of the 2004 IEEE Int. Conf. on Robotics and Automation*, pp. 3596-3601, New Orleans, April 2004.

[19] N. Metni, T. Hamel, and F. Derkx, "Visual Tracking Control of Aerial Robotic Systems With Adaptive Depth Estimation," *Proc. of the IEEE Conf. on Decision and Control*, pp. 6078-6084, Dec. 2005.

[20] N. Metni, T. Hamel, and I. Fantoni, "Visual Servoing With Orientation Limits of a X-4 Flyer," *European Control Conference*, Cambridge, UK, Sept. 2003.

[21] A. Palomino, P. Castillo, I. Fantoni, R. Lozano, and C. Pégard, "Control Strategy Using Vision for the Stabilization of an Experimental VTOL Aircraft Setup," *IEEE Trans. on Control Systems Technology*, Vol. 13(5), pp. 847-850, Sept. 2005.

[22] P. Pounds, R. Mahony, J. Gresham, P. Corke, and J. Roberts. "Towards Dynamically-Favourable Quad-Rotor Aerial Robots," *Proc. of the 2004 Australasian Conf. on Robotics and Automation*, Dec. 2004.

[23] H. Romero, R. Benosman, and R. Lozano, "Stabilization and Location of a Four Rotor Helicopter Applying Vision," *Proc. of the American Control Conference*, pp. 3930-3935, June 2006.

[24] M. W. Spong, and M. Vidyasagar, *Robot Dynamics and Control*, John Wiley and Sons, ISBN: 047161243, 1989.

[25] S. Stolle, and R. Rysdyk, "Flight Path Following Guidance for Unmanned Air Vehicles With Pan-Tilt Camera for Target Observation," *Digital Avionics Systems Conference*, Vol. 2, Oct. 2003.